RSC Advances

ROYAL SOCIETY OF CHEMISTRY

www.rsc.org/advances

Cow dung-derived nitrogen-doped carbon as a cost effective, high activity, oxygen reduction electrocatalyst

Zheng Zhang[1], Hao Li[2],Yixin Yang[1], Julian Key[3], Shan Ji[3**], Yuanyuan Ma[1], Hui Wang[1], Rongfang Wang[1,*]

[1] Key Laboratory of Eco-Environment-Related Polymer Materials, Ministry of Education of China, College of Chemistry and Chemical Engineering, Northwest Normal University, Lanzhou 730070, China

[2] Department of Chemical Engineering, Huizhou University, Huizhou, Guangdong 516007, China

[3] South African Institute for Advanced Materials Chemistry, University of the Western Cape, Cape Town 7535, South Africa

Abstract: N-doped carbon materials are promising metal-free catalysts for the oxygen reduction reaction (ORR) in fuel cells. However, their practical application depends on both significant cost reduction (by using low-cost precursors) and further improvement of their catalytic activity. Herein, we report a low-cost and scalable synthesis procedure to prepare a highly active N-doped carbon ORR catalyst using only cow dung as sources of carbon and nitrogen. The obtained catalyst produced high ORR activity comparable to commercial Pt/C in 0.1 M KOH solution regarding both ORR onset potential and half-wave potential, and had excellent tolerance to

R.F. Wang (*): wrf38745779@126.com, Tel./fax: +86-931-7971533

S. Ji (**): sji@uwc.ac.za, Tel./fax: +27-21-9599316

methanol crossover as well as stable ORR cycling performance. Furthermore, the use of cow dung puts a source of greenhouse gas pollutant to good use as an ORR catalyst for clean energy production in fuel cells.

Keywords: Nitrogen-doped carbon; Cow dung; Electrocatalyst; Oxygen reduction reaction; Fuel cells

1. Introduction

Fuel cells that operate on the oxidation of molecules such as methanol, ethanol and hydrogen hold great promise to provide clean energy for the future. However, at present, the high-cost of Pt-based catalysts, required for both the anodic oxidation of the fuel and the cathodic oxygen reduction reaction (ORR), holds back large scale implementation of such fuel cells. While the performance of Pt-based catalysts provides a bench mark[1], considerable progress has been made in developing alternative ORR catalysts derived from more abundant and/or cheaper materials[2,3]. Various novel noble-metal-free electrocatalysts with high ORR electrocatalytic activity and high stability against poisoning have begun to emerge from the research[4,5]. In particular, N-containing carbon materials stand out due to their high methanol/CO tolerance, outstanding durability, and their considerably high electrocatalytic activity[6-8].

In general, N-containing carbon materials have been fabricated by two routes: doping N directly into carbon material during synthesis, and post-treatment of carbon

materials with a nitrogen-containing precursor. However, in most cases, complex procedures, tedious post-treatments and/or expensive equipment are necessary. Recently, a number of studies have investigated different forms of biomass as precursors for preparing N-containing carbon materials for ORR catalysts, such as soya beans[4], chitosan[6] and okara[9]. Biomass can significantly reduce the overall production cost and simplify the process by offering the advantage of intrinsically high N content without the need for its external introduction. For example, recently, hair (a commonly discarded biomass material), was used to prepare heteroatom-doped carbon of high ORR activity[10].

In our local area of Gansu province, cattle rearing is a major industry that produces large quantities of cow dung as a by-product. Cow dung contains many organic compounds including crude protein, crude fat and a variety of amino acids. These organic compounds can be used as the precursors for synthesising nitrogen-containing carbon. Recent work of Bhattacharjya and Yu reported that cow dung-derived carbon exhibited high specific capacitance and durability[11]. In our previous work, waste chicken bone was used to prepare N-doped carbon of high ORR catalytic activity[12]. In the present work, we used cow dung as an extremely low cost precursor for preparing an N-containing carbon ORR catalyst. To further enhance its catalytic activity, SiO_2 particles were used as a porogen, and Fe was used as a dopant according to our previous work[13,14]. The as-prepared porous Fe-doped N-containing carbon produced higher ORR catalytic activity than commercial carbon-supported Pt catalyst, and had greater performance stability.

2. Experimental

2.1. Preparation of catalysts

Cow dung from a local farm (Lan Zhou farm) was cut into small pieces and dried at 60 ^{o}C for 12 h. Three different catalysts were made from the dried starting material. Firstly, the catalyst was prepared by carbonization 2 g of dried cow dung at 800 ^{o}C for 2 h in N_2 atmosphere. The carbonized cow dung (denoted as CD) was ball milled for 6 h and then treated in 10 mL 28 M HF solution and 10 mL 2 M HNO_3 for 24 h with stirring respectively, then filtered and washed in deionized water until the filtrate was pH 7, and then finally dried at 60 ^{o}C for 12 h.

In order to increase the surface area of the CD, CD-Si was prepared by synthesizing CD in the presence of SiO_2-nanoparticles. Dried cow dung was ball milled for 6 h, and 2 g of the resultant powder was added to 464 mg nano-structure template of SiO_2 solid nanospheres (~35 nm diameter) in 20 mL 0.032 M $FeCl_3$ solution under stirring for 20 min. The mixture was dried to a powder at 60 ^{o}C for 6 h and heated in N_2 atmosphere first to 300 ^{o}C for 1 h and then to 900 ^{o}C for 1 h. The carbonized product was ground with a pestle and mortar, then transferred to 20 mL 28 M HF solution with 48 h stirring to dissolve the SiO_2, followed by centrifuge separation at 6500 rpm for 2 min (repeated with deionized water until the supernatant reached pH 7) and finally dried at 60 ^{o}C for 12 h.

In order to increase the number of ORR active sites in CD-Si, CD-Si/Fe was prepared by re-treating CD-Si with $FeCl_3$. CD-Si/Fe was prepared by combining 1 g of CD-Si with 1 g of $FeCl_3$ dissolved in 5 mL of deionized water, then dried at 60 ^{o}C for 12 h,

ball milled for 6 h, then heated at 800 ^{o}C for 2 h, and finally treated in HNO_3 to remove unstable Fe species. Finally, the sample was rinsed with ultrapure water until a filtrate of pH 7 was obtained, and then dried at 60 °C for 12 h.

2.3. Physical characterization

X-ray diffraction (XRD) patterns of the catalysts were recorded on a Shimadzu XD-3A (Japan) goniometer, using Cu Kα radiation operated at 40 kV and 35 mA. The sorption isotherms were obtained on a Quantachrome Autosorb-1 volumetric analyzer. Specific surface area was determined by Brunauer-Emmett-Teller (BET) and the density functional theory DFT was applied for analyzing the full range of pore size distribution. Raman spectroscopy analyses of carbon materials were carried out on a FT-Raman spectroscope (RFS 100, BRUKER) employing Nd:YAG laser wavelength of 1064 nm. Scanning electron microscopy (SEM) images were obtained on a Carl Zeiss Ultra Plus field emission scanning electron microscope. Transmission electron microscopy (TEM) measurements coupled with energy dispersive spectroscopy (EDS) were carried out on a JEM-2010 Electron Microscope (Japan) with the acceleration voltage of 200 kV. X-ray photoelectron spectra (XPS) analysis were obtained using a VGEscalab210 spectrometer fitted with Mg 300 W X-ray source.

2.4. Electrochemical characterization

Electrochemical measurements were carried out on an electrochemical work station (CHI 650d). A conventional three-electrode electrochemical cell was used

comprising a platinum wire counter electrode, an Ag/AgCl (saturated KCl solution) reference electrode, and a working electrode comprising a thin film catalyst layer mounted on a 5-mm diameter glassy carbon disc. The thin film was prepared as follows: 5 mg of catalyst was dispersed ultrasonically in 1 mL of Nafion/ethanol (20 wt.% Nafion), and 8 μL of the dispersion was transferred onto the glassy carbon disc and then air dried. Electrolyte solutions were purged with high-purity N_2 (for oxygen-free solutions) for at least 30 min before each measurement.

3. Results and discussion

Fig.1 shows SEM images of CD (carbonized dung), CD-Si (CD prepared with SiO_2 porogen) and CD-Si/Fe (CD prepared with SiO_2 porogen and Fe-dopant). All three samples comprised irregularly shaped particles in the range of 100 nm to 1000 nm, with no obvious visible difference in morphology arising from the SiO_2 and Fe treatment processes. Fig. 2a and b shows TEM images of CD-Si/Fe, and high-resolution TEM in Fig. 2c shows the presence of graphitic planes in CD-Si/Fe. The elemental composition of CD-Si/Fe analyzed by EDS (Fig. 2d) comprised mainly carbon, suggesting that Fe and Si species were removed by the leaching treatment. Due to the overlap of O and F signals, the peak at 0.5 keV could be related to O and F elements. Quantitative elemental analysis found the atomic compositional ratio of carbon to nitrogen was 95.0:3.6.

The graphitic structure of the three carbon materials was characterized by Raman spectroscopy and XRD analysis. Fig. 3a shows the Raman spectra of CD, CD-Si, and CD-Si/Fe. Two peaks at ~1300 cm^{-1} and 1600 cm^{-1} appeared in all three samples,

which correspond to the D band and G band of carbon materials respectively[15]. Generally, the D band is associated with structural defects and partially disordered structures, and the G band relates to the degree of graphitization of carbon materials[16]. Table 1 lists the peak positions and the intensity ratio of band D to band G (I_D/I_G) for the different samples. The I_D/I_G of CD was 1.041. The effect of SiO_2 porogen treatment produced an I_D/I_G of CD-Si (0.983), slightly lower than that of CD. After the additional post carbonization introduction of Fe into CD-Si, the corresponding I_D/I_G value (1.208) increased significantly, indicating that CD-Si/Fe had more defects in its graphitic structure. Similar results have also been reported in literature[17-19]. Fig. 3b shows the XRD patterns of the samples produced two peaks at ca. 23.5^o and 43^o correlating to the graphitic (002) and (100) planes respectively[11]. No other obvious peaks were observed relating to inorganic impurities, suggesting most of which were removed during the various heating and acid washing steps.

Fig. 4 shows the N_2 adsorption-desorption isotherms and the corresponding pore size distribution curves of CD, CD-Si, and CD-Si/Fe. The isotherms of the three samples (Fig. 4a) were of type Ⅳ with H_2 hysteresis, implying that all three carbon materials contained some irregular pore structures. In contrast to CD-Si and CD-Si/Fe, adsorption and desorption lines for CD did not overlap, suggesting a difference in the pore type. The obvious hysteresis loop in the curves of CD-Si and CD-Si/Fe, indicates a large amount of mesopores. These results are also supported by their pore size distribution. The pores of CD (Fig. 4b), were mainly in the microporous range (<2 nm), with a small distribution in the range of 2 nm to 6 nm. Notably, CD-Si,

had significantly more pores scattered within the mesoporous range and the size range of pores was large. This result demonstrates the role of the SiO_2 template in pore formation. However, ordered pores weren't formed, because the used SiO_2 nanoparticles were not ordered before using as templates[20]. The pore size distribution of CD-Si/Fe was similar to that of CD-Si, suggesting the later treatment with $FeCl_3$ did not obviously influence the porous structure of CD-Si. From the N_2 adsorption-desorption isotherms, the estimated BET surface area was 128.5 $m^2 g^{-1}$ for CD, 495.9 $m^2 g^{-1}$ for CD-Si, and 541.8 $m^2 g^{-1}$ for CD-Si/Fe. Meanwhile, the pore volumes of CD, CD-Si and CD-Si/Fe are 0.091 $cm^3 g^{-1}$, 0.278 $cm^3 g^{-1}$ and 0.507 $cm^3 g^{-1}$ respectively. Therefore, this indicates that the increasing BET surface area and pore volume from CD to CD-Si results from the use of the SiO_2 templates, while the increase of the BET surface area and pore volume from CD-Si to CD-Si/Fe could be derive from the removal of Fe species in CD-Si.

XPS survey spectrum analysis of CD-Si/Fe (Fig.5a) detected the presence of elements C, N, F and O, while the signals of Fe and Si were almost nonexistent, which is consistent with EDS results. High resolution XPS of Fe 2p in Fig. 5b revealed a peak at ~711.8 eV, which corresponds to Fe (III)[21,22]. No peak related to Si in the region of Si 2p appeared in the high resolution XPS spectrum shown in Fig. 5c, which agrees the EDS results. Considering ORR on carbon electrodes, it is widely considered that N atoms bound to carbon may participate directly or indirectly in the reaction. More specifically, the N bonding configuration in carbon materials is also a key factor affecting ORR activity[23,24]. Therefore, high resolution XPS analysis on

CD-Si/Fe was carried out to determine which N species the material contained (Fig. 5d). N1s peaks of CD-Si/Fe divided into four peaks at ca. 398.8 eV, 400.8 eV, 401.6 eV and 406 eV, corresponding to the pyridine N, pyrrole N, quaternary N and nitrogen oxide N respectively[13,14]. Table 2 lists the percentage of different N species detected in the CD-Si/Fe sample. Pyridine N and quaternary N are considered to be the more active species for electrocatalytic reactions[23,24].

The electrochemical behavior of CD, CD-Si, and CD-Si/Fe was investigated by cyclic voltammetry (CV) in N_2 -saturated 0.1 M KOH at a scan rate of 50 mV s^{-1} (Fig. 6). CVs of the three samples within the potential range 0.2 to -1.0 V in N_2-saturated KOH solution produced no obvious peak. CD-Si/Fe produced a quasi-rectangular voltammogram typical of high-surface-area carbons and supercapacitor material[25]. This suggests that the electrochemically accessible area of CD-Si/Fe catalyst was significantly larger than those of the other two materials, which is consistent with BET surface area results.

Rotating-disk-electrode (RDE) linear sweep voltammograms (LSVs) of CD, CD-Si, and CD-Si/Fe in O_2-saturated 0.1 mol L^{-1} KOH solution are shown in Fig. 7. For comparison, the activity of commercial Pt/C (wt.20% J.M. Corp.) is also shown in the figure. Here, the oxygen reduction current was corrected for the background current to yield ORR activity of the tested catalysts. Background curves were obtained by means of LSV in quiescent N_2-purged 0.1 mol L^{-1} KOH solution after ORR measurements. Based on LSV, the ORR onset potential is determined by the point, at which the current for oxygen reduction is first observed. CD produced relatively poor ORR

electrocatalytic activity in alkaline conditions based on its very negative onset potential and low diffusion limited current. On CD-Si, the ORR onset potential was comparable to that of CD, while the diffusion limited current increased. For RDE loaded with a thin catalyst film, the diffusion limited current is governed by the mass transport of reactants in both the solution and the catalyst film. If the diffusion within the catalyst film is much faster than that outside it, the diffusion limited current depends only on the electrode rotation rate and changes little with the type of the catalyst[26]. Therefore, at the same rotation speeds the larger diffusion limited current on CD-Si suggests that its diffusion resistance was lower than that of CD, which correlates to its larger BET surface area and porous volume. Similarly, CD-Si/Fe produced a larger diffusion limited current than CD-Si again correlating to its larger BET surface area and porous volume. Notably, the ORR onset potential on CD-Si/Fe was -0.03 V, shifting positively by 40 mV to that of CD-Si at -0.07 V. In our previous work[14,27], we found Fe doping can transform inert N species for ORR into active N species, leading to an increase of ORR active sites, resulting in enhanced ORR catalytic activity. Here, the enhanced ORR catalytic activity of CD-Si/Fe mainly derived from Fe doping, and the contribution of increased mass transfer was due to the increase of BET surface area and porous volume.

Furthermore, the ORR onset potential and diffusion limited current on CD-Si/Fe and Pt/C catalyst were similar, indicating comparable ORR activity. Table 3 further compares the activity of CD-Si/Fe catalyst in terms of the ORR onset potential with those of N-doped carbon catalysts derived from various types of biomass reported in

the literature. The table shows CD-Si/Fe was more active than NPCN[2], HC-900[10], CMT[28], FCN[29], N-OMCs-800[30], GFMC3[31], and CS-900-AC[32], but was lower than those of N-C-3 (Okara-derived carbon)[14] and Fe-CEW (chicken egg white derived carbon)[27].

To gain further insight into the ORR process on CD-Si/Fe, LSVs were carried out at rotation rates from 400 to 2500 rpm (Fig. 8). Fig. 8a shows the current density on CD-Si/Fe increased as the rotation speed increased from 400 to 2500 rpm. The transferred electron number per O_2 molecule during ORR on CD-Si/Fe was calculated by the Koutecky-Levich (K-L) equation[12,13]:

$$\frac{1}{j} = \frac{1}{j_k} + \frac{1}{B\omega^{0.5}} \qquad (1)$$

where j is the measured current density, j_k is the kinetic current density, ω is the rotation speed, B is the slope of K–L plots shown in Fig. 8b based on the equation as follows:

$$B = 0.62nF(D_{O_2})^{2/3}v^{1/6}C_{O_2} \qquad (2)$$

where n is the number of electrons transferred in the reduction of one O_2 molecule in ORR, F is the Faraday constant (F = 96485 C mol^{-1}), D_{O2} is the diffusion coefficient of O_2 in 0.1 mol L^{-1} KOH (D_{O2} = 1.9×10^{-5} cm^2 s^{-1}), C_{O2} is the bulk concentration of O_2 in the electrolyte (C_{O2} = 1.2×10^{-6} mol cm^{-3}), and v is the kinematic viscosity of the electrolyte (v= 0.01 cm^2 s^{-1}). The constant 0.2 is adopted when the rotation speed is expressed in rpm. As shown in the inset of Fig. 8b. The calculated number of transferred electrons n is 4.15, 4.17, 4.04 and 4.01 at -0.35, -0.4, -0.45, and -0.5 V respectively. These numbers were larger than 4 which is the theoretical value of the

complete oxidation of per O_2 molecule. The reason for the phenomenon, we think, is mainly derived from the error of the calculation. As we know, the process of the calculation involves many numbers, such as ω. When ω was calculated into $\omega^{-1/2}$, we selected three significant figures. K-L curves are the fitting curves, thus the error would be created. The similar numbers were presented in other reported literatures[33-36]. Although the numbers were not very accuratefigures, it could give us some valuable information. The The average being 4.09, suggests that CD-Si/Fe catalyzed ORR via a dominant 4-electron transfer pathway.

Methanol tolerance and catalyst stability over sustained operation period are two important measures of ORR catalyst performance. Tolerance to methanol crossover on CD-Si/Fe and commercial Pt/C catalysts was compared in 3 M CH_3OH + 0.1 M KOH at 30 ^oC using LSV (Fig. 9). In the presence of CH_3OH, the oxidation current for Pt/C electrodes decreased sharply, implying Pt/C catalyst had poor CH_3OH tolerance. In contrast, on CD-Si/Fe, while the ORR onset potential lowered, the oxidation current density did not change, indicating CD-Si/Fe had higher CH_3OH tolerance.

The stability of ORR catalyst activity was evaluated by long-term operation. LSV plots of CD-Si/Fe and commercial Pt/C catalyst obtained after 1 and 1000 CV cycles allowed comparison of their respective stabilities (Fig. 10). After 1000 cycles, the ORR onset potential on commercial Pt/C shifted negatively by ~40 mV compared to only 10 mV on CD-Si/Fe. In addition, the half-wave potential for commercial Pt/C shifted negatively by ~29 mV compared to only 18 mV for CD-Fe/Si. Therefore, CD-Si/Fe under the above test conditions proved a more stable ORR catalyst than the

commercial Pt/C.

4. Conclusions

N-doped carbon ORR catalysts were prepared from the low cost biomass source of cow dung with enhancements gained by preparations using SiO_2 templates and Fe-doping. The resultant CD-Si/Fe catalyst produced comparable ORR catalytic activity in 0.1 M KOH solution to that of commercial Pt/C with respect to both ORR onset potential and diffusion limited current. Furthermore, CD-Si/Fe had excellent tolerance to methanol crossover and stable ORR cycling performance, and is thus a promising non-precious metal ORR catalyst candidate for fuel cells.

Acknowledgements

The authors would like to thank the National Natural Science Foundation of China (21163018, 21363022, and 51362027) for financially supporting this work.

References

1 Y. Qiu, H. Zhang, H. Zhong and F. Zhang, *Int. J. Hydrogen Energy*, 2013, **38,** 5836-5844.

2 F. Pan, Z. Cao, Q. Zhao, H. Liang and J. Zhang, *J. Power Source*, 2014. **272,** 8–15.

3 J. Li, S. Wang, Y. Ren, Z. Ren, Y. Qiu and J. Yu, *Electrochim. Acta*, 2014, **149,** 2014 56–64.

4 T. Zhou, H. Wang, S. Ji, V. Linkov and R. Wang, *J. Power Sources*, 2014, **248,** 427-433.

5 Z. Chen, D. Higgins, A. Yu, L. Zhang and J. Zhang, *Energy Environ. Sci*., 2011, **4,** 3167-3192.

6 X. Zhao, J. Zhu, L. Liang, C. Li, C. Liu, J. Liao and W. Xing, *Appl. Catal. B*, 2014, **154-155,** 177-182.

7 G. Álvarez, F. Alcaide, P.L. Cabot, M.J. Lázaro, E. Pastor and J. Solla-Gullón, *Int. J. Hydrogen Energy*, 2012, **37,** 393-404.

8 S. Kim and S.J. Park, *Anal. Chim. Acta*, 2008, **619,** 43-48.

9 H. Yang, H. Li, H. Wang, S. Ji, J. Key and R. Wang, *J. Electrochem. Soc*., 2014, **161,** F795-F802.

10 K.N. Chaudhari, M.Y. Song and J.S. Yu, *Small*, 2014, **10**, 2625-2636.

11 D. Bhattacharjya and J.S. Yu, *J. Power Source*, 2014, **262**, 224-231.

12 H. Song, H. Li, H. Wang, J. Key, S. Ji, X. Mao and R. Wang, *Electrochim. Acta*, 2014, **147**, 520-526.

13 H. Wang, K. Wang, J. Key, S. Ji, V. Linkov, R. Wang, *J. Electrochem. Soc.*, 2014, **161**, H637-H642.

14 R. Wang, H. Wang, T. Zhou, J. Key, Y. Ma, Z. Zhang, Q. Wang and S. Ji, *J. Power Source*, 2015, **274**, 741-747.

15 Z. Xu, H. Li, G. Cao, Z. Cao, Q. Zhang, K. Li, X. Hou, W. Lia and W. Cao, *Vib. Spectrosc.*, 2014, **74,** 57-63.

16 H. Wang, H. Da, R. Wang and S. Ji, *S. Afr. J. Chem*, 2014, **67,** 33-39.

17 R. Wang, T. Zhou, H. Li, H. Wang, H. Feng, J. Goh and S. Ji, *J. Power Sources*, 2014, **261,** 238-244.

18 T. Zhou, H. Wang, K. Julian, S. Ji, V. Linkov and R. Wang, *RSC Adv.*, 2013, **3,** 16949-16953.

19 S. Yang, L. Zhi, K. Tang, X. Feng, J. Maier and K. Müllen, *Adv. Funct. Mater.*, 2012, **22**, 3634-3640.

20 J. Liang, Y. Zheng, J. Chen, J. Liu, D. Hulicova-jurcakova, M. Jaroniec and S.Z. Qiao, *Angew. Chem. Int. Ed.*, 2012, **51**, 3892-3896.

21 P. Ghods, O. B. Isgor and F. Bensebaa, *Corros. Sci*., 2012, **58,** 159-167.

22 P. Ghods, O. B. Isgor, J. R. Brown, F. Bensebaa and D. Kingston, *Appl. Surf. Sci*., 2011. **257.** 4669-4677.

23 R. Silva, D. Voiry, M. Chhowalla and T. Asefa, *J. Am. Chem. Soc*., 2013, **135,** 7823-7826.

24 D. Deng, L. Yu, X. Chen, G. Wang, L. Jin, X. Pan, J. Deng, G. Sun and X. Bao, *Angew. Chem. Int. Ed*., 2013, **52,** 371-375.

25 Z.J. Lao, K. Konstantinov, Y. Tournaire, S.H. Ng, G.X. Wang and H.K. Liu, *J. Power Sources*, 2006, **162,** 1451-1454.

26 Q. Liu, H. Zhang, H. Zhong, S. Zhang and S. Chen, *Electrochim. Acta*, 2012, **81**, 313-320.

27 K. Wang, H. Wang, S. Ji, H. Feng, V. Linkov and R. Wang, *RSC Adv*., 2013, **3**, 12039-12042.

28 Y. Ma, J. Zhao, L. Zhang, Y. Zhao, Q. Fan, X.a. Li, Z. Hu and W. Huang, *Carbon*, 2011, **49**, 5292-5297.

29 C. Zhu, J. Zhai and S. Dong, *Chem. Commun.*, 2012, **48**, 9367-9369.

30 J. Lu, X. Bo, H. Wang and L. Guo, *Electrochim. Acta*, 2013, **108**, 10-16.

31 R. Gokhale, S.M. Unni, D. Puthusseri, S. Kurungot and S. Ogale, *Phys. Chem. Chem. Phys.*, 2014, **16**, 4251-4259.

32 T. Iwazaki, R. Obinata, W. Sugimoto and Y. Takasu, Electrochem. Commun., 2009, **11**, 376-378.

33 X. Bo and L. Guo, *Phys. Chem. Chem. Phys.* 2013, **15**, 2459-2465.

34 K. S. Prasad, R. Pallela, D.-M. Kim and Y.-B. Shim, *Part. Part. Syst. Char.*, 2013, 30, 557-564.

35 H. Peng, Z. Mo, S. Liao, H. Liang, L. Yang, F. Luo, H. Song, Y. Zhong and B. Zhang, *Sci. Rep.*, 2013, **3**, 1765.

36 W. Yang, T.-P. Fellinger and M. Antonietti, *J. Am. Chem. Soc.*, 2011, **133**, 206-209.

Figures:

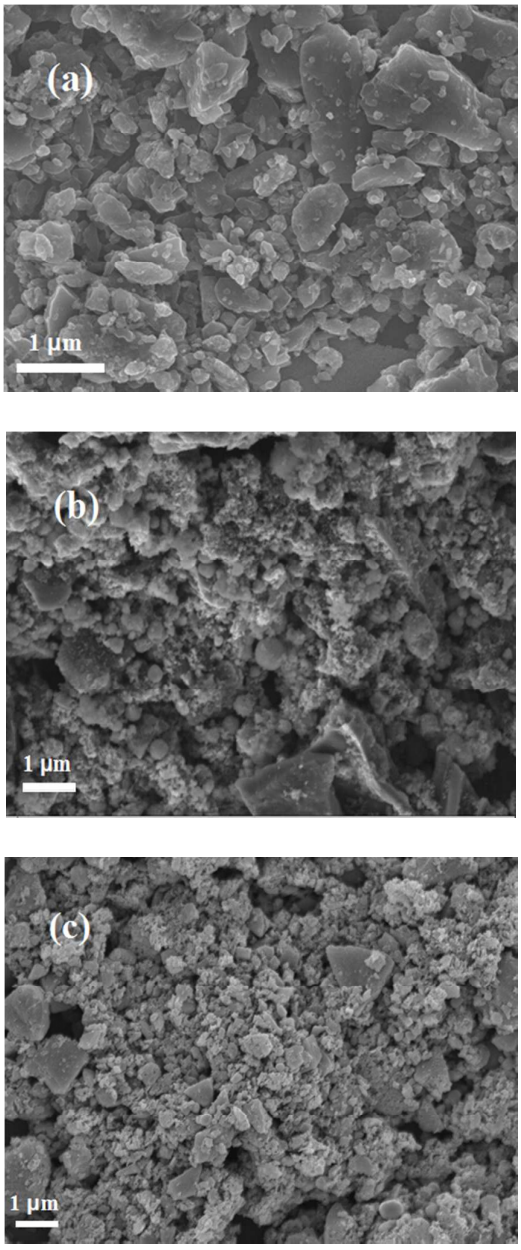

Figure 1. SEM images of CD (a), CD-Si (b) and CD-Si/Fe (c).

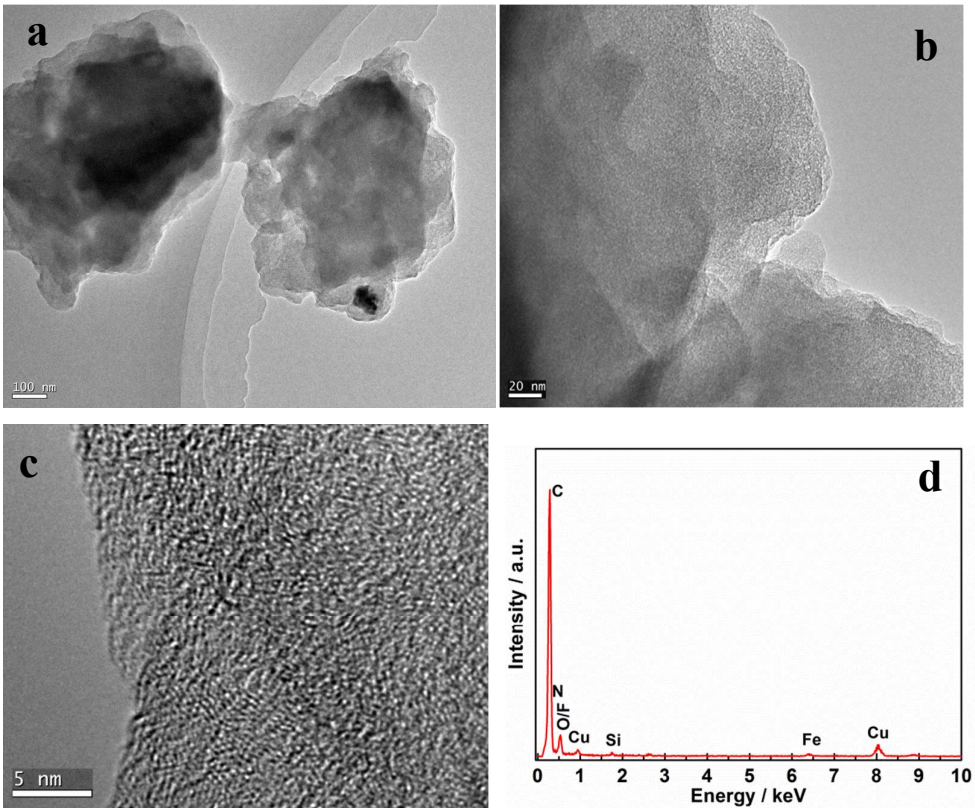

Figure 2. TEM images of CD-Si/Fe under different magnifications (a-c), and EDS pattern of CD-Si/Fe (d).

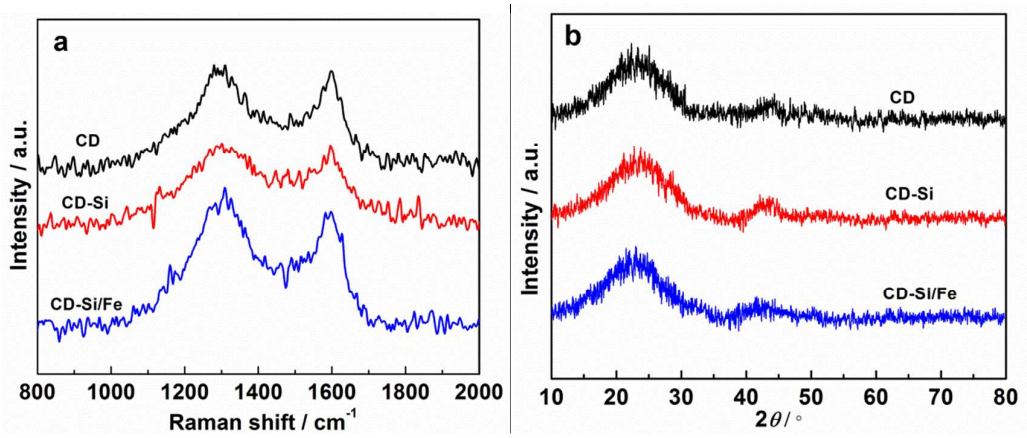

Figure 3. Raman spectra (a) and XRD patterns (b) of CD, CD-Si, and CD-Si/Fe.

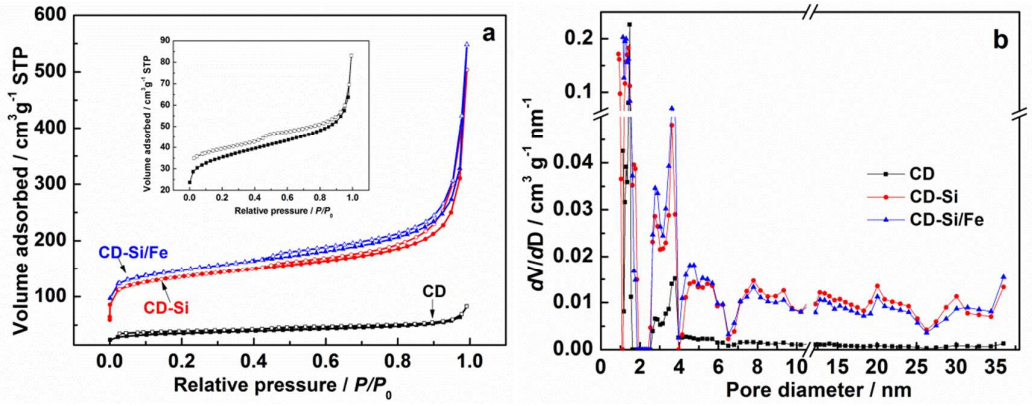

Figure 4. N_2 adsorption-desorption isotherms (a) and the corresponding pore size distribution curves (b) for CD, CD-Si, and CD-Si/Fe.

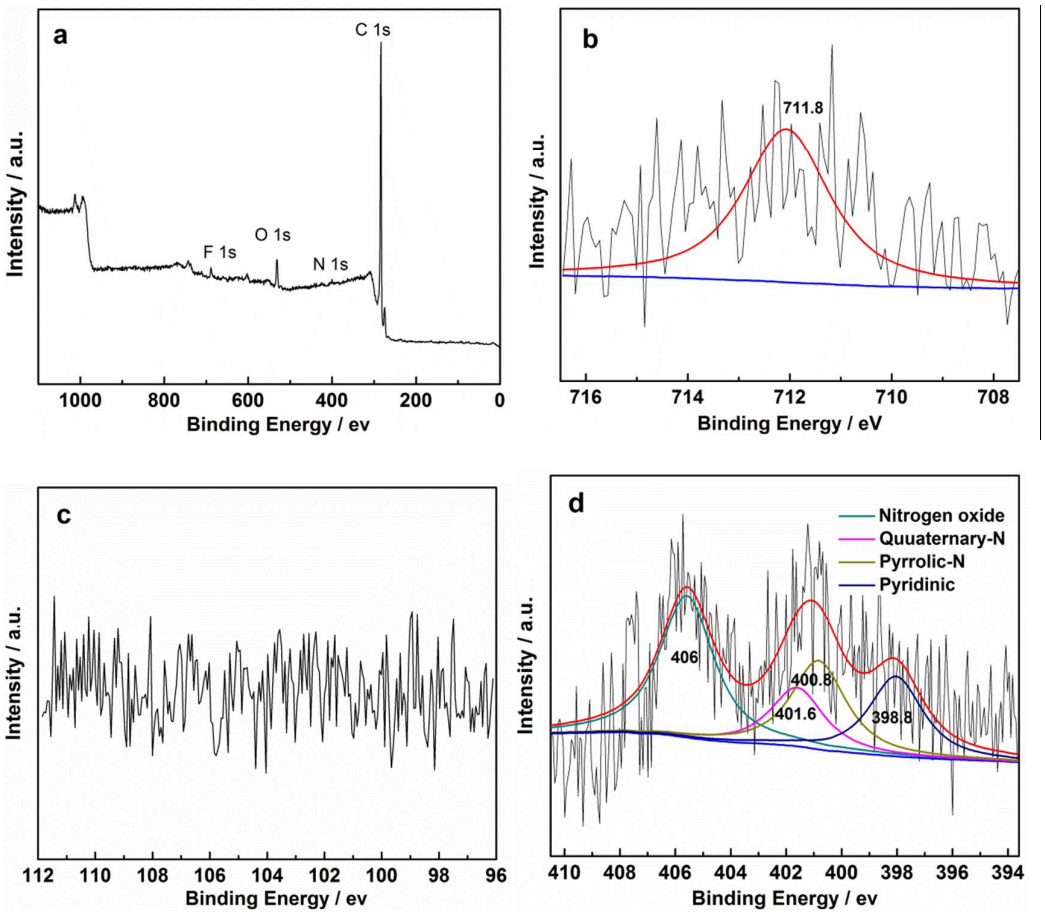

Figure 5. (a) XPS survey spectrum, (b) Fe 2p, (c) Si 2p, and (d) N 1s XPS spectrum of CD-Si/Fe.

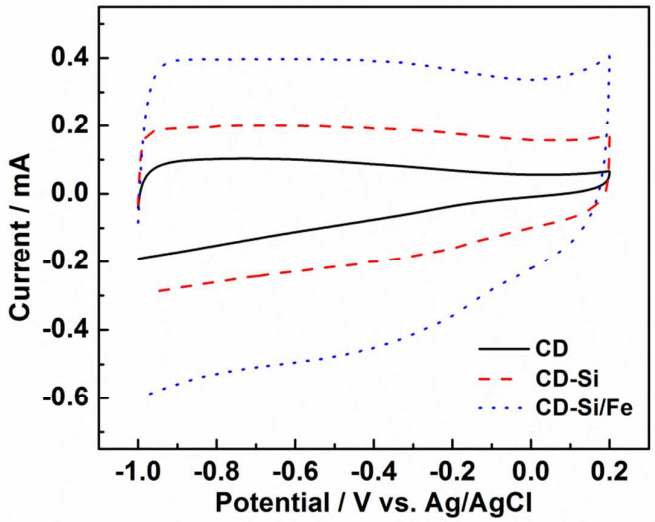

Figure 6. Cyclic voltammograms of CD, CD-Si, and CD-Si/Fe in N_2-saturated 0.1 M KOH at a scan rate of 50 mV s^{-1}.

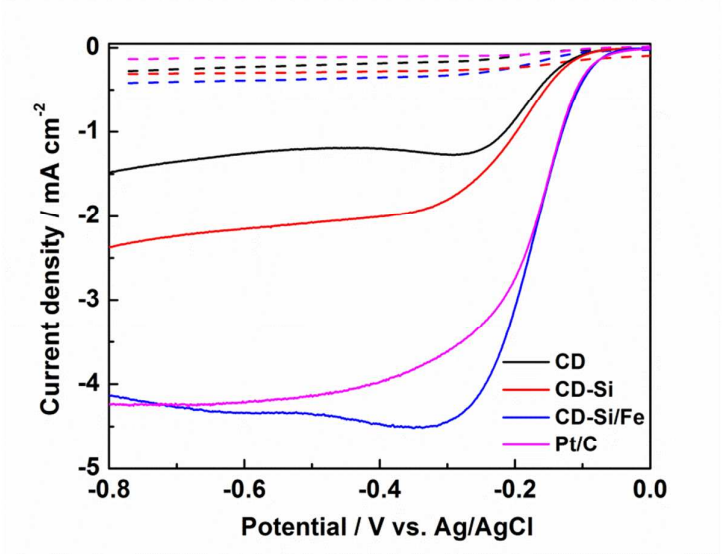

Figure 7. Linear sweep voltammograms of CD, CD-Si, CD-Si/Fe, and Pt/C in N_2 (dash lines) or O_2 -saturated (solid lines) 0.1 M KOH solution, rotation speed: 1600 rpm, and scan rate: 5 mV s^{-1}.

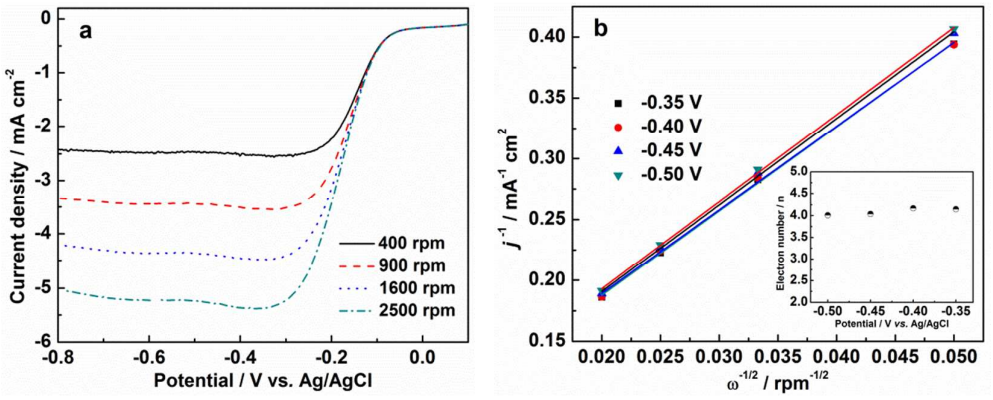

Figure 8. (a) LSVs for ORR in O_2-saturated 0.1 M KOH solution on CD-Si/Fe at various rotation rates, scan rate: 5 mV s^{-1}; (b) The K-L plots for ORR derived from (a); Inset: the number of transferred electron at different potential.

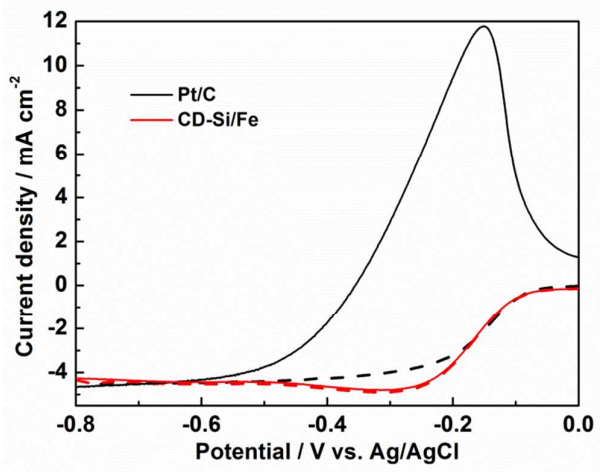

Figure 9. (a) LSVs for ORR in O_2-saturated 3 M CH_3OH + 0.1 M KOH solution on CD-Si/Fe and Pt/C electrodes, rotation speed: 1600 rpm, scan rate: 5 mV s^{-1}; for comparison, LSVs without CH_3OH (dash line with the same color).

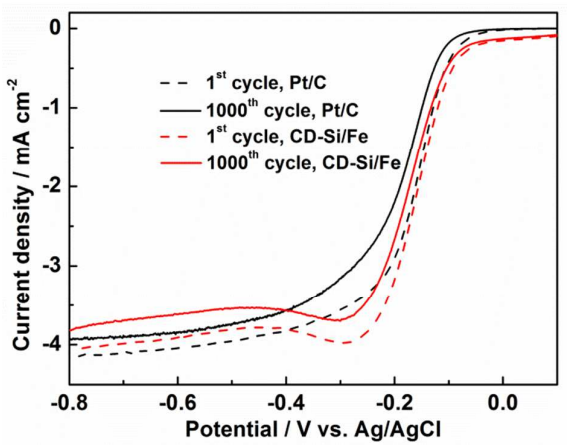

Figure 10. RDE linear sweep voltammograms recorded after the 1st and 1000th CV cycle on CD-Si/Fe and Pt/C electrodes in O_2–saturated 0.1 M KOH at a 1600 rpm rotation rate and 5 mV s^{-1} scan rate.

Table 1. Peak position of D and G bands and their intensity ratios.

	I_D/I_G	D(cm^{-1})	G(cm^{-1})
CD	1.041	1294.31	1596.84
CD-Si	0.983	1294.31	1596.84
CD-Si/Fe	1.208	1306.97	1596.84

Table 2. N configurations content in CD-Si/Fe.

Species	BE(eV)	Full width high maximum (FWHM)	Concentration (%)
Pyridinic-N	398	2.3	21.80
Pyrrolic-N	400.8	2.4	24.12
Quaternary-N	401.6	2.2	15.97
Nitrogen oxide	406	2.3	38.11

Table 3. Comparison of CD-Si/Fe ORR catalytic activity to other biomass-derived carbon catalysts considering ORR onset potential.

Sample	The type of biomass precursors	Onset potential (V vs. RHE)	Literature
CD-Si/Fe	Cow dung	0.936	-
NPCN	Dead ginkgo leave	0.900[a]	2
HC-900	Hair	0.846[a]	10
N-C-3	Okara	0.975	14
Fe-CEW	Egg white	0.976	27
CMT	Catkins	0.776	28
FCN	Soy milk	0.666[a]	29
N-OMCs-800	Honey	0.836	30
GFMC3	Gram flour	0.883	31
CS-900-AC	Silk	0.83	32

[a]The value estimated by us derived from the figure.